# EPR Studies of $Cr^{3+}$ and $Fe^{3+}$ in Host Crystals with Langbeinite Structure

J. Kastner*, B. D. Mosel, and W. Müller-Warmuth

Institut für Physikalische Chemie der Westfälischen Wilhelms-Universität, Schlossplatz 4/7, D-48149 Münster, Germany

Z. Naturforsch. **52a**, 1123–1133 (1997); received August 28, 1996

Electron paramagnetic resonance (EPR) spectra of trivalent chromium and iron ions have been investigated in host crystals of double sulfates with langbeinite structure, $A_2B_2(SO_4)_3$, with $A = NH_4^+$, $Rb^+$, $Tl^+$ and $B = Cd^{2+}$, $Mg^{2+}$. In most cases, single crystals could be grown, and the spin Hamiltonian parameters have been determined from the rotational diagrams. Powder spectra were analyzed and simulated as well. Three centres of axial symmetry with different zero field splittings have been observed for $Cr^{3+}$, and two for $Fe^{3+}$. The trivalent impurity ions have been shown to occupy divalent lattice sites substitutionally, but the environments are different depending on the structure and the mechanism of charge compensation. A qualitative description of the incorporation of dopants has been possible on this basis, taking into account the local relaxation and the ligand field stabilization effects. Temperature dependent single crystal and powder measurements have provided information on the zero field splitting and phase transitions.

## 1. Introduction

Double sulfates, isostructural with the mineral langbeinite $K_2Mg_2(SO_4)_3$, have attracted considerable interest for many reasons. Most compounds of this class undergo structural phase transitions from a paraelectric cubic phase ($P2_13$ symmetric) at room temperature to a ferroelastic orthorhombic phase ($P2_12_12_1$) at low temperatures, sometimes via ferroelectric monoclinic ($P2_1$) and triclinic phases (P1) [1–3]. Some of these materials exhibit electro-optic effects useful for the modulation of light at room temperature [4, 5].

The langbeinites can easily be doped with paramagnetic impurity ions such as $Cr^{3+}$, $Mn^{2+}$ and $Fe^{3+}$ to perform EPR studies. EPR spectroscopic data are known first of all for $Mn^{2+}$ in cadmium and magnesium langbeinites [6–12], but scarcely and not systematically for other impurity probes such as $Cu^{2+}$ [13] and $VO^{2+}$ [8]. The present paper is focused on trivalent paramagnetic ions; to our knowledge $Cr^{3+}$ has not yet been studied so far; our investigations of $Fe^{3+}$ are based on a preceding paper of Böttjer and Stockhausen [14].

$Cr^{3+}$ and $Fe^{3+}$ have the configuration $3d^3$ and $3d^5$, respectively, and the groundstates are $^4F$ and $^6S$. $S = 3/2$ and $S = 5/2$ EPR systems are formed. For $Cr^{3+}$, spin-orbit and spin-spin couplings lead to two Kramers' doublets with $m_s = \pm 3/2, \pm 1/2$; for $Fe^{3+}$ there are three Kramers' doublets which split in the magnetic field into six Zeeman levels. Three and five allowed EPR transitions, respectively, can be observed, whose resonances depend on the orientation of the crystal in the magnetic field. Considering the symmetry of the sites of the paramagnetic ions in the langbeinites, the crystal field splitting of $Cr^{3+}$ was expected to be describable by one ZFS (zero field splitting) parameter ($B_2^0$), that of $Fe^{3+}$ by four parameters ($B_2^0$, $B_4^0$, $B_4^{\pm 3}$).

In the present paper we studied six compounds doped with $Cr^{3+}$ and three doped with $Fe^{3+}$ aiming a systematic investigation of langbeinites with trivalent impurity ions. Information as incorporation, defect structure, symmetry of various centres and charge compensation was expected. It should be possible to study relationships between spin Hamiltonian parameters, crystal structure and ionic radii. Temperature dependent data should give EPR information on phase transitions.

## 2. Experimental

### 2.1 Crystal Growth and Sample Preparation

Crystals of the double sulfates $A_2B_2(SO_4)_3$ with $A = NH_4^+$, $Rb^+$, $Tl^+$ and $B = Cd^{2+}$, $Mg^{2+}$ were grown either by evaporation from aqueous solutions

* Present address: Sachtleben Chemie GmbH, Dr.-Rudolf-Sachtleben-Str. 4, D-47198 Duisburg.

Reprint requests to Prof. W. Müller-Warmuth.

0932-0784 / 96 / 1000-1123 $ 06.00 © – Verlag der Zeitschrift für Naturforschung, D-72072 Tübingen

of the corresponding $A_2SO_4$ and $BSO_4$ compounds or from the melt (Bridgeman-Stockbarger method). The procedures were similar to those described in [12]. Cadmium langbeinites could be obtained as single crystals of sufficient size and quality; powder samples were prepared for all the materials. Special attention had to be paid to $Mn^{2+}$ impurities which could only be avoided by extremely pure solutions. For that purpose, the crystals were doped with $Cr^{3+}$ and $Fe^{3+}$ using solutions of elemental chromium (99.995%) and iron (99.98%), respectively, in sulfuric acid free of manganese. The $Cr^{3+}$ and $Fe^{3+}$ concentrations are between 0.05 and 2 mol%. Optimum amounts which guarantee a sufficient signal-to-noise ratio of the EPR spectra without line broadening were tested experimentally. The dopants did not influence the morphology. All those crystals doped with $Cr^{3+}$ had to be annealed for several hours at temperatures between 570 K and 630 K.

Most crystals were found to grow with large $\langle 111 \rangle$ faces. The samples were mounted adequately in the EPR cavity and could be rotated about axes according to the morphology of the crystal. Information could also be obtained from powder spectra since the point symmetry of the defects appeared to be sufficiently high.

### *2.2 EPR Spectroscopy*

The EPR mesurements were made on a conventional Bruker X-band spectrometer (ESP 300) in the range from 9.33 to 9.78 GHz depending on sample and measuring device. The microwave frequency was determined using a piceine standard ($g = 2.0041(1)$). The spectrometer was furthermore equipped with a NMR gaussmeter and a refrigeration system. Two Pt-100 resistors were used for either driving the temperature control system or measuring the temperature at the sample site.

Single crystals were studied at various orientations by measuring the spectra in steps of 2° when rotating about an $c^*$-axis parallel to the $\langle 111 \rangle$ direction and about an $a^*$-axis perpendicular to this. The axes denoted by an asterisk may differ slightly from the directions of the real $c$- and $a$-axes. Small misorientations could be corrected in the course of the fitting procedure. The whole procedure was computer driven and fully automated. The data were transferred to appropriate computers and further manipulated using various home-made programs for the search of signals, integration, correction and construction of rotational diagrams [15].

The observed data were fitted to the spin Hamiltonian [16]

$$\hat{H} = \mu_B \hat{\mathbf{S}} \tilde{g} \mathbf{B} + \sum_{n=2}^{2S} \sum_{m=-n}^{n} B_n^m \hat{\mathbf{O}}_n^m \qquad (1)$$

with the Stevens operators $\hat{\mathbf{O}}_n^m$ [17], the Bohr magneton $\mu_B$ and the magnetic field $\mathbf{B}$.The principal values of the $\tilde{g}$ tensor and the ZFS parameters $B_n^m$ have to be derived from the spectra. The fitting program included a matrix diagonalization followed by a least-squares fit of the field positions for the two rotations with the fitting parameters $g_x, g_y, g_z, B_n^m$ and the crystal orientation in the laboratory system (misorientation).

## 3. Results

### *3.1 $A_2Cd_2(SO_4)_3:Cr^{3+}$ with $A = NH_4$, Rb, Tl*

Single crystals were grown from all these materials and both rotational diagrams and powder spectra were measured. Figure 1 shows an example of the angular dependences of the single crystal EPR spectra characteristic of these three compounds. The rotational diagram about $a^*$ reveals that the magnetic $z$ axis coincides with the threefold crystal ($c^* \parallel \langle 111 \rangle$) axis. From the diagram about $c^*$ it can be concluded that there are three different paramagnetic centres with axial symmetry, each consists of four symmetry spectra. Two rotational diagrams of measurements about axes perpendicular to each other are therefore sufficient to describe the EPR properties.

It can be furthermore recognized from the spectra that the zero field splittings are of the same order of magnitude as the Zeeman splitting in the magnetic field. The strong magnetic field limit cannot be applied to simplify the description of the EPR spectra. In addition to the lines which originate from $Cr^{3+}$, in the field range between 310–370 mT signals from $Mn^{2+}$ impurities are observable. These will not be considered further.

The orientation of the crystal was determined within the fitting procedure, i.e. misorientations of up to 1 or 2° in terms of the Eulerian angles were found and included in the simulation program. As a result of the simulation, which is also shown in Fig. 1, the ZFS parameters of Table 1 were obtained for the three axial centres. The intensity ratio of the centres $Cr_1:Cr_2 \cdot Cr_3$ turned out to be 30:1:2. For

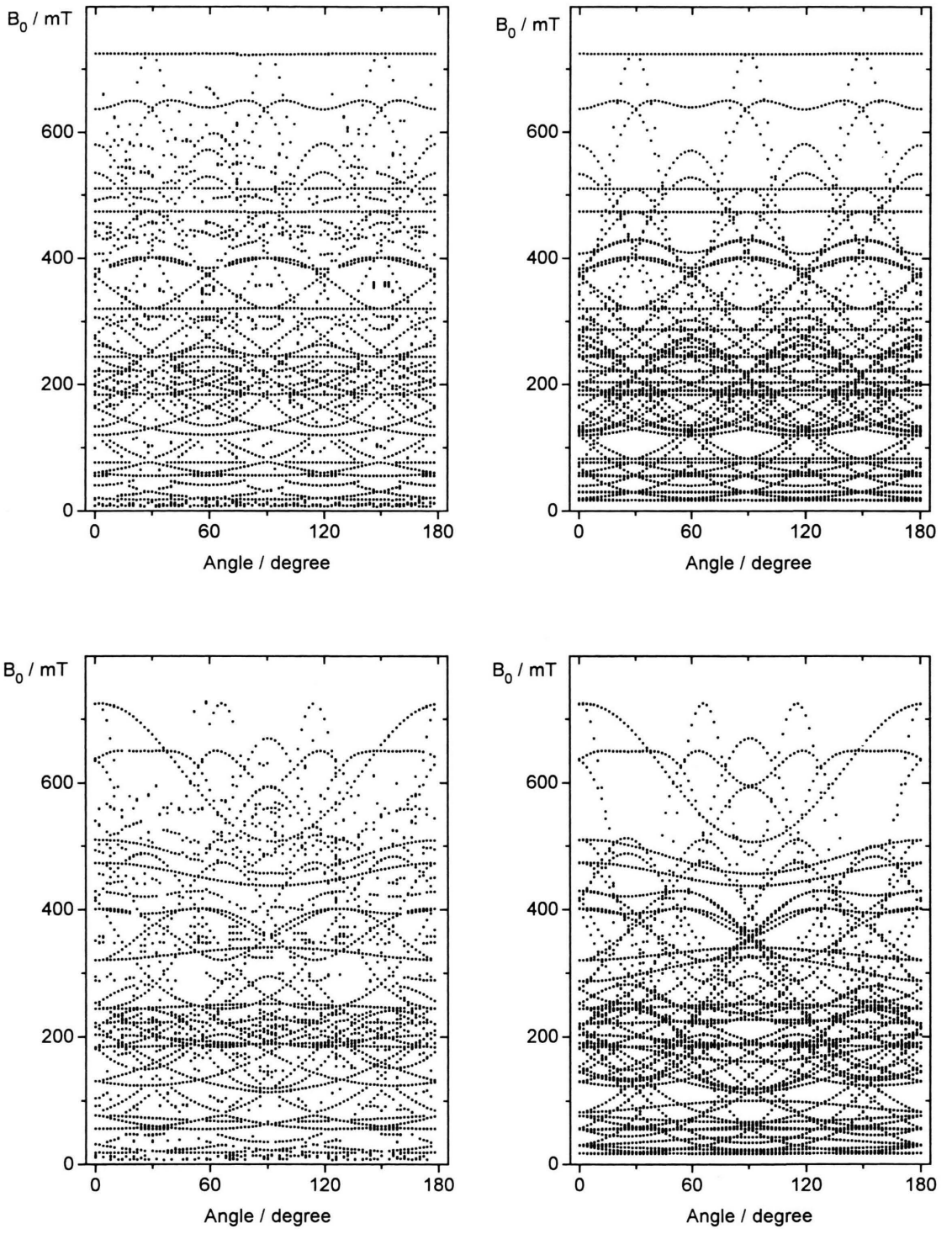


Fig. 1. Measured (left) and simulated (right) rotational diagrams for $Cr^{3+}$ in $Tl_2Cd_2(SO_4)_3:Cr^{3+}$ at 9.760 GHz and room temperature. The diagrams at the top belong to a rotation about the $c^*$-(parallel to the threefold $\langle 111 \rangle$) axis, those at the bottom to a rotation about $a^* \perp c^*$.

Table 1. Zero field splitting (ZFS) parameters observed at room temperature for the three paramagnetic centres with axial symmetry in langbeinites doped with $Cr^{3+}$. Centre no. 1 has the largest intensity. The random errors are indicated by the values in parentheses. Data obtained from powder rather than single crystal spectra are marked by an asterisk.

| Compound | | $\lvert B_2^0 \rvert$/GHz | | |
|---|---|---|---|---|
| A | B | Centre 1 | Centre 2 | Centre 3 |
| $NH_4$ | Cd | 1.334 (7) | 1.524 (9) | 3.223 (4) |
| Rb | Cd | 0.977 (7) | 1.355 (5) | 3.577 (9) |
| Tl | Cd | 1.115 (6) | 1.474 (9) | 3.805 (9) |
| $NH_4$ | Mg | 1.162 (3)* | 1.418 (5)* | 4.348 (3)* |
| Rb | Mg | 1.237 (5) | 1.662 (8) | 4.970 (7) |
| Tl | Mg | 1.369 (6)* | 1.833 (6)* | 5.738 (2)* |

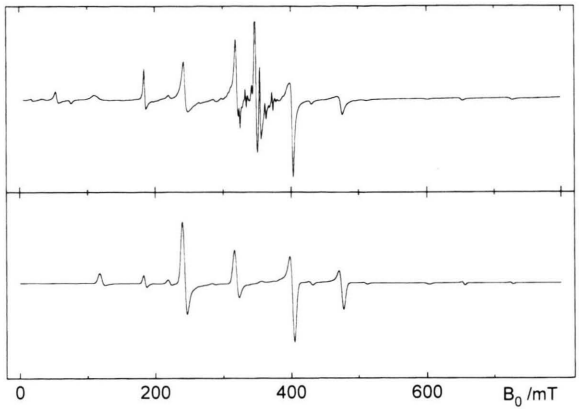


Fig. 2. EPR-powder pattern of $Tl_2Cd_2(SO_4)_3:Cr^{3+}$ at 300 K and a microwave frequency of 9.769 GHz (top). The simulation of this spectrum is shown at the bottom; the central part belonging to $Mn^{2+}$ impurities was not simulated.

$Rb_2Cd_2(SO_4)_3:Cr^{3+}$ and $(NH_4)_2Cd_2(SO_4)_3:Cr^{3+}$ it was 10:1:1 and 20:1:1, respectively. We do not present the $g$ values in detail, because they are all rather similar. Both $g_{\parallel}$ and $g_{\perp}$ are close to 1.97 for all three $Cr^{3+}$ centres in each compound. The widths of the single lines in the spectrum amount to about 3 mT for the $NH_4$ and Tl compounds, and to 6 and 7 mT for the Rb compound.

Assignment of the line positions of powder spectra becomes complicated for two reasons. First of all, the strong field limit is no longer valid, and secondly because of the occurrence of three types of defect centres. It was, however, possible to simulate the essential features using the general information on EPR spectra of $Cr^{3+}$ in langbeinites obtained from the single crystal measurements. Figure 2 shows as an example the powder spectrum of the same compound and its simulation. The EPR parameters derived from such spectra appear to be the same within the error limits, but not quite so accurate.

Temperature dependent measurements were also carried out. The spectra may change completely if structural changes occur. The EPR spectrum of $Tl_2Cd_2(SO_4)_3:Cr^{3+}$ at liquid nitrogen temperatures (Fig. 3) leads for example, to two defect centres of lower symmetry rather than three axial centres. $B_2^0$ is 1.895(5) GHz and 1.629(7) GHz for these centres, and $B_2^2$ equals 0.447(8) GHz and 0.765(9) GHz, respectively. Analyzing the spectra between 370 K and 77 K, two phase transitions can be identified for the thallium compound, one at 126 K and the other one at 96 K. Figure 4 shows the evolution of the spectra in the whole temperature range.

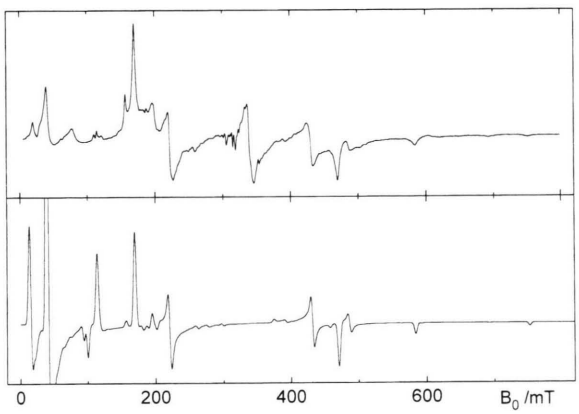


Fig. 3. Powder spectrum of $Tl_2Cd_2(SO_4)_3:Cr^{3+}$ at 77 K and a microwave frequency of 9.34 GHz. Its simulation at the bottom.

Corresponding studies of $(NH_4)_2Cd_2(SO_4)_3:Cr^{3+}$ resulted in one observable phase transition near 90 K, whereas for $Rb_2Cd_2(SO_4)_3:Cr^{3+}$ no dramatic change of the spectra was found. Smooth changes within the room temperature phases can be explained by the temperature dependence of the ZFS parameters. In all cases $\lvert B_2^0 \rvert$ increases linearly with temperature. This linear dependence could be established in detail for the three centres in $(NH_4)_2Cd_2(SO_4)_3:Cr^{3+}$ between 200 K and 370 K, and for the compounds with Rb and Tl between 150 K and 370 K.

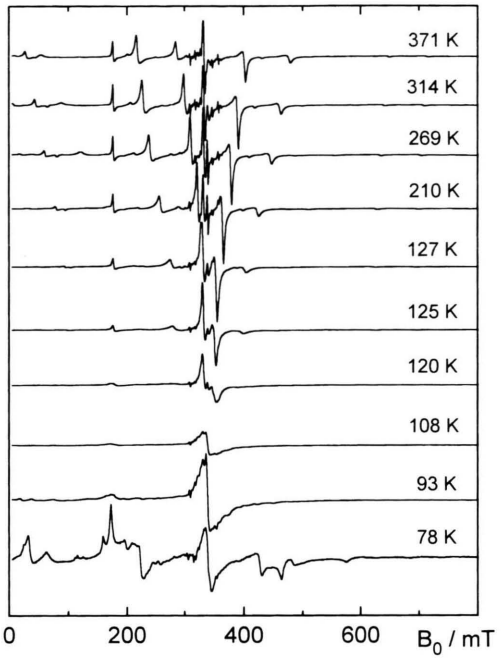


Fig. 4. EPR powder patterns of $Tl_2Cd_2(SO_4)_3:Cr^{3+}$ between 78 K and 371 K.

### *3.2 $A_2Mg_2(SO_4)_3:Cr^{3+}$ with A = $NH_4$, Rb, Tl*

On the whole, the spectra look similar for this class of compounds. However, single crystals could only be grown for $Rb_2Mg_2(SO_4)_3:Cr^{3+}$. Therefore, for the other two materials only powder patterns were analyzed. In all cases, again three axial defect centres could be identified and their zero field splitting parameters are listed in Table 1 as well. All the $g$ values are again not far from 1.97. But, in addition to the three axial defects, at least in one compound we observed an additional centre with lower symmetry. The temperature dependence of the spectra was studied down to 77 K, but no indications of phase transitions were found. The linear dependence of $B_2^0$ on temperature could be confirmed within the whole range between 77 K and 370 K.

### *3.3 $A_2Cd_2(SO_4)_3:Fe^{3+}$ with A = $NH_4$, Rb, Tl*

Previous measurements of $Fe^{3+}$ doped langbeinites [14] revealed one centre of axial symmetry, but Mössbauer studies in similar compounds doped with $Fe^{2+}$ and $Fe^{3+}$ resulted in two different types of defects [18]. Our present studies were therefore focused on the search for further centres. Both single crystal and powder spectra were studied.

As an example of rotation diagrams, in Fig. 5 we show again those of the Tl compound, but now doped with trivalent iron. We recognize two centres of axial symmetry with strongly different zero field splittings. For centre no. 1, the width of the spectra extends from 40 to 660 mT, that for centre no. 2 only from about 300 to 400 mT. The magnetic axes of both centres coincide with the crystal axes. Simulation leads to the four ZFS parameters listed in Table 2. $g$ is nearly isotropic and amounts to 2.003 (centre no. 1) and 2.004 (centre no. 2). The EPR spectra of $Fe^{3+}$ in the $NH_4$ and Rb langbeinites display rather similar features characteristic of two axial centres as well. The ZFS parameters are again given in Table 2. The signs of the ZFS parameters were determined from the temperature dependence of the intensity of selected EPR transitions. The intensity ratios of the occurrence of centres no. 1 and no. 2 turned out to be 1:3, 1:4 and 1:5, respectively, for the compounds with $NH_4$, Rb and Tl.

Figure 6 shows the temperature dependence of a single crystal spectrum for fixed orientation. Upon decreasing the temperature, one recognizes that new signals appear at 86 K which are not yet visible at 89 K. At lower temperatures, the new signals increase at the expense of those of the two axial centres. For $Rb_2Cd_2(SO_4)_3:Fe^{3+}$ phase transitions can be identified in the ranges 123–127 K and 97–100 K from an increase of the number of signals by lowering of the symmetry of the paramagnetic centres. Phase transitions near 127 K, 120 K and 94 K were observed for the thallium langbeinite.

Within the high temperature phase the ZFS parameters proved to be temperature dependent, but the behaviour was not the same as that for $Cr^{3+}$ centres. For the first $Fe^{3+}$, $|B_2^0|$ increases as for the $Cr^{3+}$ centres, but for centre no. 2 it decreases. The linear ranges are more limited. The temperature dependence of $B_4^0$ was studied as well; in all cases there was a decrease of $|B_4^0|$ at elevated temperatures.

## 4. Discussion

### *4.1 Incorporation of Trivalent Ions*

Both $Cr^{3+}$ and $Fe^{3+}$ form defect centres in the langbeinite structure with axial symmetry. Since the magnetic $z$ axis appears to be parallel to the threefold

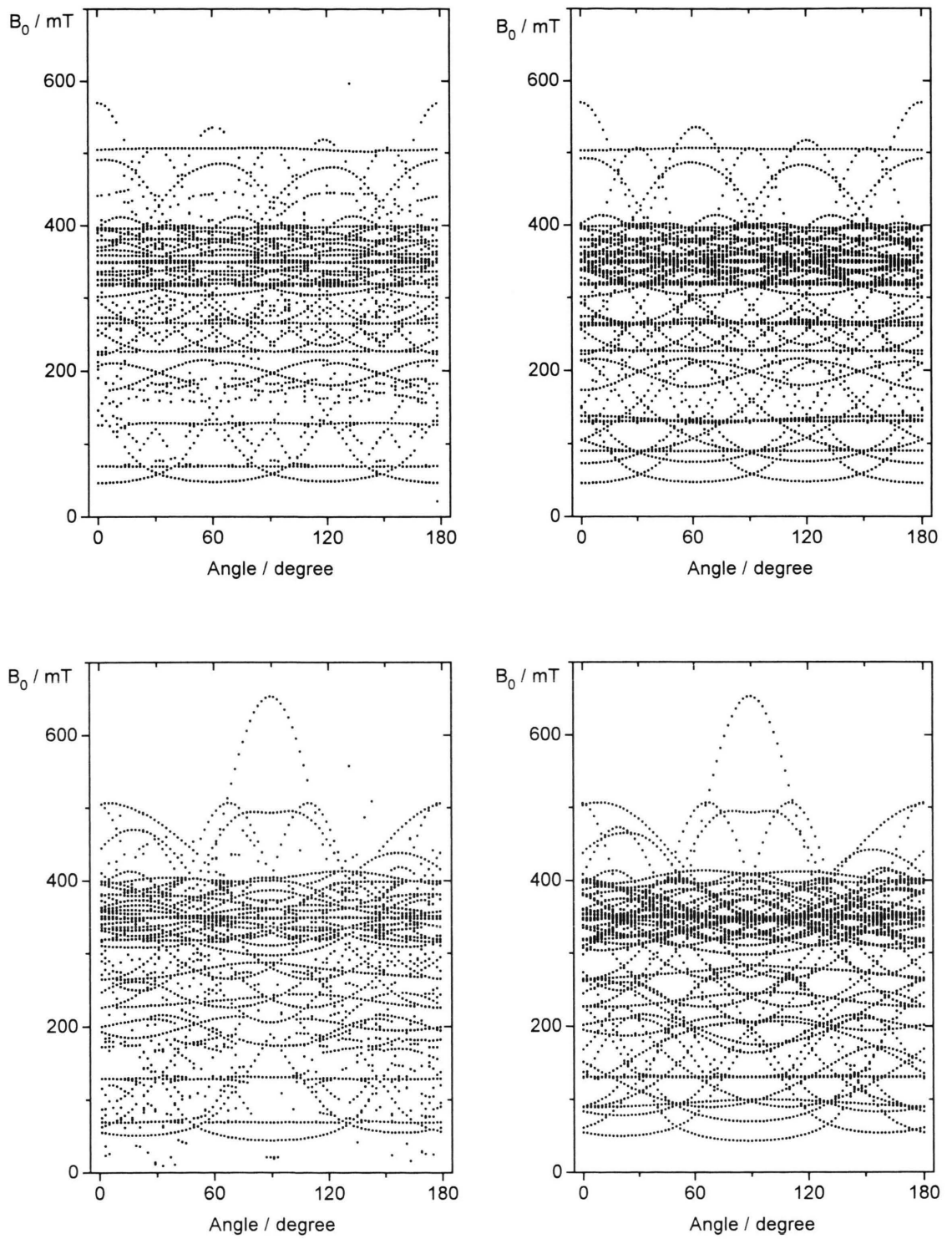


Fig. 5. Same as Fig. 1, but for $Tl_2Cd_2(SO_4)_3:Fe^{3+}$.

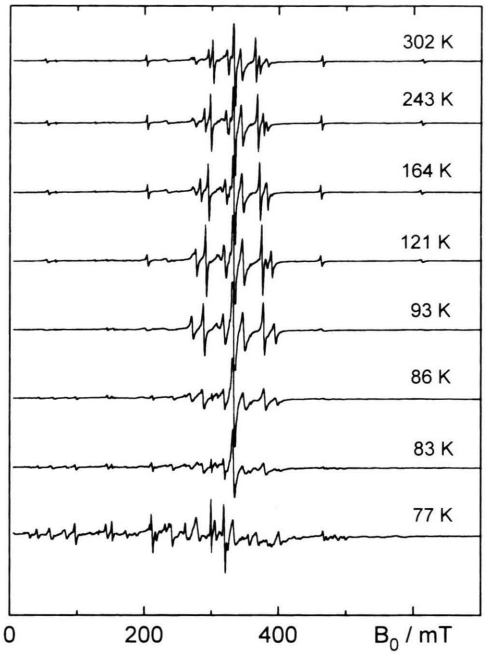


Fig. 6. Single crystal EPR spectra of $Fe^{3+}$ in $(NH_4)_2Cd_2(SO_4)_3:Fe^{3+}$ at various temperatures and a microwave frequency of 9.35 GHz. The sample is oriented with its $c^*$-axis parallel to $B_0$.

crystal axis the dopant ions must be located along the body diagonal of the unit cell. Occupation of monovalent lattice sites in place of the much larger $A^+$ ions is extremely improbable and would lower the symmetry. For geometrical reasons interstitial sites may be ruled out as well, so that the assumption of an incorporation of the trivalent paramagnetic ions in place of the crystallographically non-equivalent $B^{2+}$ sites is reasonable. The substitution of trivalent $Cr^{3+}$ and $Fe^{3+}$ ions is therefore similar to that of divalent $Mn^{2+}$ [6–12, 14], but the mechanism of charge compensation has to be considered further. The ionic radii [19] of $Cr^{3+}$ (61.5 pm) and $Fe^{3+}$ (64.5 pm) are somewhat smaller than those of $Mg^{2+}$ (72.0 pm) and $Cd^{2+}$ (95.0 pm) whereas that of $Mn^{2+}$ (83.0 pm) is larger. Further support of the substitution model is obtained from the dependences of the ZFS parameters.

Assignment of the defect centres to the non-equivalent $B^{2+}(1)$ and $B^{2+}(2)$ sites of the crystal structure is not possible solely from EPR since both sites possess axial symmetry. But we know the separation between ligands and central ion and the different distortions of the first coordination sphere from crystal structure refinements of $(NH_4)_2Cd_2(SO_4)_3$ [7] and $Rb_2Cd_2(SO_4)_3$ (within the frame of this work). It appears first of all that the situation in the various compounds is similar. Lattice site B(1) with its oxygen environment displays a more important deviation from the octahedral symmetry than B(2), for which a larger volume is available.

The Newman superposition model (SPM), on the other hand, provides a method to relate the observed zero field splittings to the position of the ligands in the first coordination shell of the paramagnetic defect [20–22]. A "distortion function" $V_z$ can be calculated from the geometry using empirical relations and known parameters for $Cr^{3+}$ and $Fe^{3+}$ with oxygen ligands [23, 24]. $V_z$ turns out to be negative for both $Cr^{3+}$ and $Fe^{3+}$ at both sites B(1) and B(2). Its (absolute) amount is clearly larger for paramagnetic ions at B(1) sites. Within the frame of the SPM, the main ZFS parameter is then obtained from

$$B_2^0 = \bar{B}_2 V_z \tag{2}$$

with an so-called intrinsic parameter $\bar{B}_2$ characteristic of the host crystal.

Comparison of the observed $B_2^0$ values with the geometrical data and the SPM analyses leads for $Cr^{3+}$ to the conclusion that centre 1 of Table 1 can be assigned to the B(2) site and centre 2 to B(1). Centre 3 with the much larger ZFS splitting will be discussed further below in connection with the charge compensation mechanism. Corresponding arguments hold for the incorporation of trivalent iron ions. Here it seems that the (new) centre no. 2 can be assigned to the larger B(2) site, whereas centre no. 1 may be compared with the $Cr^{3+}$ centre no. 3.

### *4.2 Zero Field Splittings*

It is worth-while to consider the crystal field splitting parameters and their dependences on the various compounds in more detail. First of all, the SPM provides a guess of the sign of the main ZFS parameter $B_2^0$, even for those cases where the sign could not be determined experimentally as for the $Cr^{3+}$ dopants (Table 1). The intrinsic parameter $\bar{B}_2$ and its sign is known from $V_z$ calculations and experimental $B_2^0$ data (cf. Eq. (2)) for many similar systems [23, 25, 26] and within the frame of the present work for several $Fe^{3+}$ doped langbeinites (Table 2). It has turned out to be nearly exclusively positive. We may conclude that the sign of $B_2^0$ is most likely negative for the $Cr^{3+}$ doped

Table 2. Zero field splitting parameters observed at room temperature for the two axial paramagnetic centres in cadmium langbeinites single crystals doped with $Fe^{3+}$. The random errors are indicated by the values in parentheses. The sign of the parameters was determined experimentally in most cases; some signs (in parentheses) were only suggested.

| Cd-Compound | $B_2^0$/GHz | | $B_4^0/10^{-4}$ GHz | | $B_4^3/10^{-3}$ GHz | | $B_4^{-3}/10^{-3}$ GHz | |
|---|---|---|---|---|---|---|---|---|
| A | Centre 1 | Centre 2 | Centre 1 | Centre 2 | Centre 1 | Centre 2 | Centre 1 | Centre 2 |
| $NH_4$ | −0.643 (3) | (−)0.106 (1) | −6.2 (5) | (+)8.6 (5) | 6.2 (5) | (−)7.2 (4) | −1.7 (2) | (−)2.0 (2) |
| Rb | −0.696 (4) | (−)0.089 (4) | −6.4 (1) | (+)8.4 (6) | 6.3 (9) | (−)10 (2) | −1.7 (2) | (−)0.2 (9) |
| Tl | −0.701 (3) | −0.136 (2) | −6.1 (2) | 8.5 (7) | 6.8 (3) | −6.8 (6) | −1.6 (3) | −2.1 (3) |

langbeinites as well. Negative signs were also found for the ZFS splitting parameters of $Mn^{2+}$ doped langbeinites, at least proved for the most intensive defect [12].

Similarities between $Cr^{3+}$, $Fe^{3+}$ and $Mn^{2+}$ dopants exist as well if the dependences on the langbeinite composition are considered. Inspection of Table 1 and comparison with the ionic radii of the monovalent (A) and divalent (B) cations [19] shows that $|B_2^0|$ appears to be a linear function of the ratio $Q = r_B/r_A$ of the ionic radii for all three centres (Figure 7). This behaviour, at least that of centres no. 1 and no. 2, is comparable with what was found for $Mn^{2+}$ dopants [12]. $B_2^0$ of centre no. 3 displays a more pronounced dependence on $Q$ and occupies a special position as already mentioned in the last paragraph.

As far as the result for $Fe^{3+}$ dopants are concerned the more intense centres no. 1 with the larger splitting correspond to those already known from the previous paper [14]. Figure 8 shows the dependence on $Q$ with the data of [14] included. The identification of centre no. 2 is only possible for single crystals of high quality. Due to the small crystal field splitting the signal separation in the spectrum is delicate and may be complicated by $Mn^{2+}$ impurities. Spectra analysis reveals that the fourth order ZFS parameters $B_4$ must not be neglected; but there is no systematic relation to the composition of the host crystal.

Inspection of the $B_2^0$ values of $Mn^{2+}$, $Fe^{3+}$ and $Cr^{3+}$ probes and their slopes as a function of $Q$ shows that both the absolute values and the composition dependence have the tendency to increase in this order from manganese to chromium. Within one probe both $Mn^{2+}$ centres and $Cr^{3+}$ centres no. 1 and no. 2 behave similar. $Fe^{3+}$ centre no. 1 and $Cr^{3+}$ centre no. 3 are distinguished by larger splittings and more important dependences on composition.

The size and the composition dependence of the ZFS mirrors the distortion of the environment of the $B$ site occupied by the paramagnetic probe. Depending on the composition in detail the coordination shell may be contracted or expanded, but without influenc-

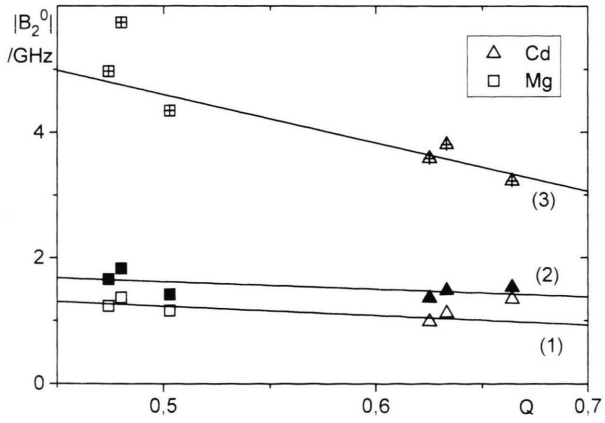


Fig. 7. ZFS parameter $B_2^0$ of the three $Cr^{3+}$ centres in various langbeinite crystals as a function of $Q = r_B/r_A$, the ratio of the ionic radii of the divalent and monovalent cations.

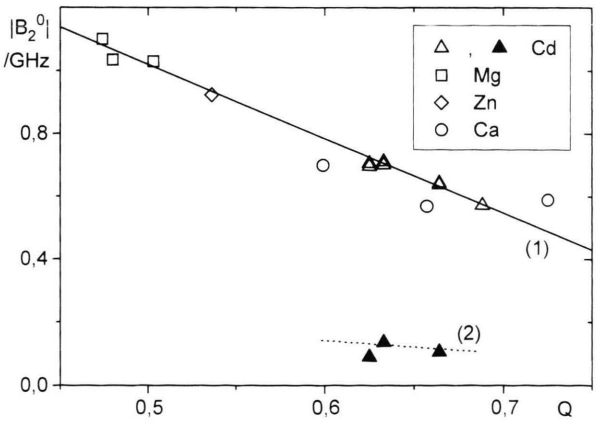


Fig. 8. Same as Fig. 7, but for the two $Fe^{3+}$ centres. The extra bold points are from this work, the other points for centre no. 1 are taken from [14].

ing the symmetry. SPM analysis does not explain the $Q$ dependence since the local structure relaxation has to be considered in addition.

As proposed by Böttjer et al. [12], the surrounding oxygens can relax towards the centre of the defect if $B^{2+}$ is substituted by a smaller cation such as $Mn^{2+}$. Such a relaxation will result in a reduced distortion of the octahedral ligand shell and may explain the differences of $B_2^0$ for $Mn^{2+}$ (both centres) and $Fe^{3+}$ (centre no. 2) and the dependence on the size of the host cation $B^{2+}$.

This relaxation model holds for paramagnetic $^6S$ groundstate ions. For $Cr^{3+}$ with its $^4F$ groundstate, the effect of ligand stabilization has to be considered in addition. If there are three d electrons instead of five, only the favoured $t_{2g}$ orbitals are occupied and not the two $e_g$ orbitals with higher energy. A stabilization can then be achieved by the ligand field. Local relaxation and ligand field stabilization act in the opposite directions and this may explain the larger $B_2^0$ values for $Cr^{3+}$ dopants.

The modified relaxation model may also account for the observed largely different occupation numbers of the crystallographically non-equivalent B(1) and B(2) centres. For the $3d^5$ ions $Mn^{2+}$ and $Fe^{3+}$, by relaxation site B(2) is greatly favoured. The intensity ratios are 200:1 to 500:1 for $Mn^{2+}$ in favour of this site [12] whereas for $Fe^{2+}$ only this site was found to be occupied. The $3d^3$ ion $Cr^{3+}$, on the other hand, is exposed to both relaxation and ligand field stabilization and the occupation difference is less (2:1 to 30:1).

### *4.3 Charge Compensation*

Incorporation of trivalent dopants such as $Cr^{3+}$ and $Fe^{3+}$ at divalent B sites requires the compensation of the positive excess charge. In principle, the following mechanisms are imaginable: (i) compensation in the first ligand shell, (ii) incorporation of impurity anions at interstitial sites, (iii) substitution of $B^{2+}$ by $A^+$ at B sites or (iv) unoccupied $A^+$ positions, all in the vicinity of the defect. Compensation at larger distances from the paramagnetic centres would be another possibility (v).

Item (i) may be immediately excluded because an additional charge at oxygen or sulfate ions would reduce the symmetry. (ii) is likewise inprobable since we obtained the same EPR spectra of crystals either prepared from solutions (with $OH^-$ and $HSO_4^-$ ions available) or from the melt. Addition of small monovalent anions did not influence the spectra as well [14]. (iii) would not retain the symmetry because of the size effect, so that we are left with (iv) and (v). Considering the $B_2(SO_4)_3^{2-}$ lattice structure with the monovalent ions in the cavities, removal of a certain number of $A^+$ would not change the overall structure greatly. Charge compensation in the immediate vicinity of an defect will expand the first ligand shell and increase $B_2^0$; compensation at larger distances does not effect the ligand sphere greatly.

The various observed centres may therefore be thought to arise from different charge compensation mechanisms. The $Cr^{3+}$ centre no. 3 and the $Fe^{3+}$ centre no. 1 with their large zero field splittings and important dependences on the ratio $Q$ of the ionic radii may be caused by near-by $A^+$ vacancies. For the other defects large distance compensation is suggested as for $Cr^{3+}$ doped $CsMgCl_3$, $CsMgBr_3$ and $CsCdBr_3$ [27].

### *4.4 Temperature Dependent Behaviour*

Three different effects of the temperature dependence may be considered: the steady variation of $B_2^0$ (and other ZFS parameters), the occurrence of phase transitions and the EPR properties of low temperature phases. Apart from the exemplified discussion of the spectrum of Fig. 3 in paragraph 3.1, spectroscopy of low temperature phases is not the subject of the present study. This subject was treated in another recent paper of this Institute, at least for $Mn^{2+}$ dopants [28].

Within the cubic ($P2_13$) room temperature phase the linear increase of $B_2^0$ ($Cr^{3+}$) with $T$ is similar in all langbeinites and for all three types of paramagnetic centres; the order of magnitude amounts to 1 MHz/K. $B_2^0$ of the $Fe^{3+}$(1) centre behaves similarly, but for centre no. 2 $B_2^0$ decreases. The ZFS parameter $B_4^0$ decreases at elevated temperatures for both iron centres (order of magnitude: $10^{-4}$ MHz/K). For $Mn^{2+}$ centres a different behaviour was observed [12, 28]: very little dependence of $B_2^0$ on temperature far away from a phase transition and exponential dependence near the transition point.

Discussing such temperature dependences we may distinguish between implicit effects, caused by the influence of temperature on the volume of the crystal, and explicit effects by the interaction of the groundstate with excited states via lattice vibrations [29]. If a phase transition is approached precursory effects may be added.

Distinction between implicit and explicit effects from the EPR data only is not possible. But because of the different behaviour of $Mn^{2+}$, $Cr^{3+}$ and $Fe^{3+}$ and in view of the sign of the temperature variation of $B_2^0$ the conclusion may be drawn that explicit effects dominate.

Phase transitions can be recognized by abrupt changes of the spectra and the EPR parameters if they are connected with changes of the local environments of the $Cr^{3+}$ and $Fe^{3+}$ probes. Intense signals may disappear and others emerge. Furthermore, upon decreasing the temperature the total width of the spectra becomes reduced and it is useful to consider the sudden increase of individual linewidths. Sometimes it was difficult to determine the transition temperature because the quality of the spectra and the signal-to-noise ratio diminished. Table 3 shows phase transition temperatures for cadmium langbeinites doped with $Cr^{3+}$ or $Fe^{3+}$ which were determined within the frame of this work and assigned to transitions from the cubic room temperature phase to the monoclinic, triclinic and orthorhombic phases. No phase transitions at all were observed in magnesium langbeinites although some are known from dielectric, dilatometric and heat capacity measurements [30–32].

Comparison of the transition temperatures of Table 3 with those known from $Mn^{2+}$ probes [8–11] and a $^{57}Fe$ Mössbauer study [18], or from dielectric [33–39], dilatometric [31] optical [35, 40], Raman [41], heat capacity [32, 42–44], X-ray [36, 45], elastic [36, 37, 39], pyroelectric [38, 39] measurements of the pure langbeinites shows that the data are all similar and that there is practically no influence of the dopants. Among the various models proposed to explain the phase transitions [2, 8, 46, 47], in agreement with the previous $Mn^{2+}$ study [28] our experiments are in favour of the model of octahedral distortion [2]. On decreasing the temperature the distortion of the $B^{2+}$-oxygen octahedra increases until a less symmetric arrangement becomes more stable thermodynamically. This could also explain the dramatic increase of the linewidth when approaching the transition by lattice softening.

Table 3. Phase transition temperatures as observed from the temperature dependence of EPR. n.o. means: no transition observed within the investigated temperature range; n.e.: evaluation not possible.

| Compound | | | Observed Phase Transition Temperature in K | | |
|---|---|---|---|---|---|
| A | B | Defect | $P2_13 \rightarrow P2_1$ | $P2_1 \rightarrow P1$ | $P1 \rightarrow P2_12_12_1$ |
| $NH_4$ | Cd | $Cr^{3+}$ | 90 (1) | n.o. | n.o. |
| $NH_4$ | Cd | $Fe^{3+}$ | 87 (2) | n.o. | n.o. |
| Rb | Cd | $Cr^{3+}$ | n.e. | n.e. | n.o. |
| Rb | Cd | $Fe^{3+}$ | 125 (3) | 98 (2) | n.o. |
| Tl | Cd | $Cr^{3+}$ | 126 (1) | n.e. | 96 (1) |
| Tl | Cd | $Fe^{3+}$ | 127 (1) | 120 (3) | 94 (1) |


[1] G. Gattow and J. Zeeman, Z. Anorg. All. Chemie **293,** 233 (1958).
[2] D. Speer and E. Salje, Phys. Chem. Minerals **13,** 17 (1986) and references therein.
[3] T. Hikita, M. Kitabatake, and T. Ikeda, J. Phys. Soc. Japan **49,** 1421 (1980) and references therein.
[4] C. F. Buhrer, L. R. Bloom, and D. H. Baird, Appl. Optics **2,** 839 (1963).
[5] C. F. Buhrer and L. Ho, Appl. Optics **3,** 314 (1964).
[6] I. Tatsuzaki, J. Phys. Soc. Japan **17,** 1312 (1962).
[7] H. N. Ng and C. Calvo, Can. J. Chem. **53,** 1449 (1975).
[8] D. S. Babu, G. S. Sastry, M. D. Sastry, and A. G. I. Dalvi, J. Phys. C **17,** 4245 (1984).
[9] S. K. Misra and S. Z. Korczak, J. Phys. C **19,** 4353 (1986).
[10] S. K. Misra and S. Z. Korczak, Solid State Commun. **61,** 665 (1987).
[11] S. K. Misra and S. Z. Korczak, J. Phys. C **20,** 4485 (1987).
[12] T. Böttjer, G. Lehmann, and M. Stockhausen, Z. Naturforsch. **47a,** 849 (1992).
[13] V. C. Mouli and G. S. Sastry, J. Mol. Structure **96,** 163 (1982).
[14] T. Böttjer and M. Stockhausen, Phys. Stat. Sol. (B) **174,** 359 (1992).
[15] T. Behner, Thesis (1991) and T. Böttjer, Thesis (1991), Universität Münster, unpublished.
[16] A. Abragam and B. Bleaney, Electron Paramagnetic Resonance of Transition Ions, Clarendon Press, Oxford 1970.
[17] K. W. H. Stevens, Proc. Phys. Soc. **A 65,** 209 (1952).
[18] M. Windhaus, Thesis (1996), Universität Münster.
[19] R. D. Shannon, Acta Cryst. **A 32,** 751 (1976).
[20] D. J. Newman, Adv. Phys. **20,** 197 (1971).
[21] D. J. Newman and W. Urban, Adv. Phys. **24,** 793 (1975).
[22] D. J. Newman and B. Ng, Rep. Progr. Phys. **52,** 699 (1989).
[23] R. Büscher and G. Lehmann, Chem. Phys. Lett. **124,** 202 (1986).
[24] F. Prissok, Thesis, Münster 1989, unpublished.
[25] K. A. Müller and W. Berlinger, J. Phys. C **16,** 6861 (1983).
[26] V. K. Jain, and G. Lehmann, Solid State Commun. **71,** 523 (1989).
[27] G. L. McPherson and K. O. Devaney, J. Phys. C **13,** 1735 (1980).
[28] T. Böttjer and M. Stockhausen, Z. Naturforsch. **51a,** 1084 (1996).
[29] W. M. Walsh, J. Jeener, and N. Bloembergen, Phys. Rev. A **139,** 1338 (1965).
[30] T. Hikita, H. Sekiguchi, and T. Ikeda, J. Phys. Soc. Japan **43,** 1327 (1977).

[31] M. Kahrizi and M. O. Steinitz, Solid State Commun. **66,** 375 (1988).
[32] J. I. Artman and J. Boerio-Goates, Ferroelect. **132,** 141 (1992).
[33] F. Jona and R. Pepinsky, Phys. Rev. **103,** 1126 (1956).
[34] H. Ohshima and E. Nakamura, J. Phys. Chem. Solids **27,** 481 (1992).
[35] M. Glogarova and J. Fousek, Phys. Stat. Sol. (a) **15,** 579 (1973).
[36] T. Ikeda and G. Yasuda, Japan. J. Appl. Phys. **14,** 1287 (1975).
[37] T. Hikita, T. Kudo, Y. Chiubachi, and T. Ikeda, J. Phys. Soc. Japan **41,** 349 (1976).
[38] N. Yamada, J. Phys. Soc. Japan **46,** 561 (1979).
[39] M. Maeda, J. Phys. Soc. Japan **49,** 1090 (1980).
[40] B. Brezina and M. Glogarova, Phys. Stat. Sol. (a), **11,** K 39 (1972).
[41] S. Kreske and V. Devarajan, J. Phys. C **15,** 7333 (1982).
[42] V. Franke, M. Glogarova, and E. Hegenbarth, Phys. Stat. Sol. (b), **58,** K 69 (1973).
[43] V. Franke, E. Hegenbarth, and B. Brezina, Phys. Stat. Sol. (a), **28,** K 77 (1978).
[44] H. Cao, N. K. Dalley, and J. Boerio-Goates, Ferroelect. **146,** 45 (1993).
[45] N. Yamada and S. Kawano, J. Phys. Soc. Japan **43,** 1016 (1977).
[46] F. Lissalde, S. C. Abrahams, S. L. Bernstein, and K. Nassau, J. Appl. Phys. **50,** 845 (1979).
[47] N. Yamada, M. Maeda, and H. Adachi, J. Phys. Soc. Japan **50,** 907 (1981).